IEEE Access
Multidisciplinary : Rapid Review : Open Access Journal

Received 11 March 2024, accepted 2 April 2024, date of publication 5 April 2024, date of current version 15 April 2024.

Digital Object Identifier 10.1109/ACCESS.2024.3385498

RESEARCH ARTICLE

Low-Voltage Mixed-Mode Analog Filter Using Multiple-Input Multiple-Output Operational Transconductance Amplifiers

MONTREE KUMNGERN[1], **FABIAN KHATEB**[2,3,4], **AND TOMASZ KULEJ**[5]

[1]Department of Telecommunications Engineering, School of Engineering, King Mongkut's Institute of Technology Ladkrabang, Bangkok 10520, Thailand
[2]Department of Microelectronics, Brno University of Technology, 601 90 Brno, Czech Republic
[3]Faculty of Biomedical Engineering, Czech Technical University in Prague, 272 01 Kladno, Czech Republic
[4]Department of Electrical Engineering, Brno University of Defence, 662 10 Brno, Czech Republic
[5]Department of Electrical Engineering, Czestochowa University of Technology, 42-201 Czestochowa, Poland

Corresponding author: Montree Kumngern (montree.ku@kmitl.ac.th)

This work was supported by the University of Defence Brno within the Organization Development Project Vojenské autonomní a robotické systémy (VAROPS).

ABSTRACT This paper presents a novel mixed-mode, low-power, 1 V analog filter that uses multiple-input multiple-output operational transconductance amplifiers (MIMO-OTAs). This filter uses four OTAs, two grounded capacitors, and one grounded resistor and offers four modes, namely voltage, current, transconductance, and transimpedance modes. Each mode of operation provides non-inverting and inverting low-pass, high-pass, band-pass, band-stop, and all-pass filter transfer functions (10 transfer functions). Thus, in four operating modes, the designed filter offers 40 transfer functions, which is the full capability of a mixed universal filter. The natural frequency of all filter functions can be electronically controlled. To obtain the multi-input OTA, the multiple-input bulk-driven MOS transistor (MIBD-MOST) technique is used. This technique can reduce the number of MOS input differential pairs and the supply voltage. The active mixed-mode filter was simulated using a CMOS TSMC 0.18 μm process in the Cadence Virtuoso ADE Suite. The simulation results confirm the performance of the proposed filter.

INDEX TERMS Active filter, mixed-mode filter, operational transconductance amplifier, low-power circuit, analog circuit.

I. INTRODUCTION

Low-voltage and low-power integrated circuits are an extremely challenging topic for researchers nowadays as low supply voltages and very low power consumption are required for modern portable electronics, biomedical devices and sensors. Minimal circuit power consumption can reduce the size of the device and can also save battery lifetime (for recharging). Portable and wearable devices utilize active filters to filter the out-of-band interference and noise (low-pass filter), select desired signals (band-pass filter), or reject 50 Hz power line interference (band-pass filter).

The associate editor coordinating the review of this manuscript and approving it for publication was Harikrishnan Ramiah.

Universal filters are circuits that can usually realize five standard filtering responses in the same circuit. These are the low-pass filter (LPF), high-pass filter (HPF), band-pass filter (BPF), band-stop filter (BSF), and all-pass filter (APF). Regarding the nature of input and output signals, universal filters are classified as current-mode (CM), voltage-mode (VM), transadmittance-mode (TAM), and transimpedance-mode (TIM). In a VM filter, both input and output signals are voltages; in a CM filter, both input and output signals are currents; in a TAM filter, input signals are voltages and output signals are currents; in a TIM filter, input signals are currents and output signals are voltages. Therefore, a mixed-mode filter is a versatile and flexible circuit. Many mixed-mode filters have been introduced using variant active devices such as current feedback operational amplifiers (CFOAs) [1], [2],

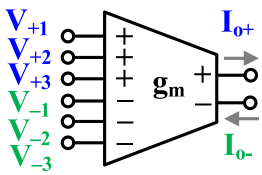

FIGURE 1. Electrical symbol of the MIMO-OTA.

second-generation current conveyors (CCIIs) [3], [4], and differential difference current conveyors (DDCC) [5], [6]. However, these mixed-mode filters do not provide electronic tuning capabilities.

The operational transconductance amplifier (OTA) is a basic building block of analog and mixed signal circuits. This active building block is a voltage controlled current source because the differential input voltage produces an output current by using its transconductance gain (g_m). Thus, OTA-based circuits usually do not require passive resistors. Many mixed-mode universal filters using OTAs as active devices have been reported [7], [8], [9], [10], [11]. However, these mixed-mode universal filters are rather high-power consumption. Low-voltage low-power mixed-mode universal filters have been proposed in [12], [13], [14], [15], and [16]. However, these mixed-mode universal filters do not provide full capability of mixed-mode universal filters, namely each VM, CM, TAM, and TIM does not provide both non-inverting and inverting transfer functions of LPF, HPF, BPF, BSF, and APF.

The input and output signals in the voltage and/or current forms of mixed-mode filters can offer some advantages in the design of modern integrated circuit systems. For example, some applications in integrated circuits may require a connection between voltage-mode circuits and current-mode circuits. The TAM, which has a voltage input and a current output, or TIM, which has a current input and a voltage output, can be used to convert between voltage and current modes [17]. In addition, the availability of both non-inverting and inverting output signals may be advantageous for connection to the next stages without additional circuit requirements, such as non-inverting or inverting amplifiers. Thus, mixed-mode filters, which support input and output signals as voltage or current and provide both non-inverting and inverting filtering functions, are valuable subjects of research and development for various filtering applications compatible with modern integrated circuit systems.

This paper presents a new multiple-input multiple-output (MIMO) mixed-mode active filter employing three multiple-input OTAs (MI-OTAs), one multiple-input multiple-output OTA (MIMO-OTA), two grounded capacitors, and one grounded resistor. Both non-inverting and inverting second-order LPF, HPF, BPF, BSP, APF can be obtained in VM, CM, TIM, and TAM by selecting appropriate input and output signals. Thus, the proposed mixed-mode filter offers 40 transfer functions in a single topology. The natural frequency of all filtering functions can be electronically controlled. The input voltages and output currents possess a high impedance. To the best of the authors' knowledge, a mixed-mode filter operating similarly to this proposed filter is not available in the literature, likely due to the use of circuits based on multiple-input and multiple-output OTAs. The proposed filter was simulated and designed using the Cadence Virtuoso ADE Suite and 0.18 μm CMOS technology from TSMC.

II. PROPOSED CMOS TOPOLOGY OF THE MIMO-OTA

Fig. 1 shows the symbol of the 3-input MIMO-OTA. Its ideal input and output characteristics can be determined by the formula:

$$I_{o+} = -I_{o-} = g_m \left(V_{+1} + V_{+2} + V_{+3} - V_{-1} - V_{-2} - V_{-3}\right) \tag{1}$$

where g_m is the transconductance gain, V_{+j} and V_{-j} are the non-inverting and inverting input voltages ($j = 1, 2, 3$), and I_{o+} and I_{o-} are the output currents.

Fig. 2 shows the CMOS schematic of the proposed MIMO-OTA. The circuit consists of the linearized differential input stage (transistors M_1-M_2, biased by the current sources realized by the transistors M_3 and M_4), and two folded cascode output stages M_5-M_{12} and M_{5c}-M_{12c}, which organize the high-impedance outputs I_{o+} and I_{o-}. To realize the multiple inputs of the OTA, the input transistors M_1 and M_2 were replaced by multiple-input bulk-driven transistors shown in Fig. 3 (the so-called MIBD-MOST technique [18], [19]).

A capacitive voltage divider/voltage summing circuit is created by the capacitors C_{Bi}. The capacitors are shunted by very large resistances R_{MOSi}, created by an anti-parallel connection of two minimum-size MOS transistors operating in the cutoff region. The additional resistors provide proper biasing of the MOS transistor's bulk-terminal for dc. Using the capacitive voltage divider instead of multiplied input stages simplifies the overall structure and saves power. For frequencies much larger than $f_c = 1/C_{Bi}R_{MOSi}$, the transfer function from a single differential input V_{+i}-V_{-i} to the bulk terminals of M_1 and M_2, (V_{b1}-V_{b2}), can be expressed as:

$$\frac{V_{b1}(s) - V_{b2}(s)}{V_{+i}(s) - V_{-i}(s)} = \frac{C_{Bi}}{C_\Sigma} = \beta_i \tag{2}$$

where $C_\Sigma = C_{B1}+C_{B2}+C_{B3}+C_{ib}$, and C_{ib} is the input capacitance of the differential stage, seen from its bulk terminals. Note that full symmetry of the input stage has been assumed.

For three inputs, and assuming $\beta_1 = \beta_2 = \beta_3 = \beta$ and C_{ib} is much smaller than the capacitances of the input divider, we obtain $\beta = 1/3$; thus, the AC signal is attenuated three times. In this case, the differential signal at the bulk terminals of the input transistors M_1 and M_2 can be expressed as:

$$\beta V_{b1}(s) - V_{b2}(s) = \begin{pmatrix} V_{+1}(s) - V_{-1}(s) + V_{+2}(s) \\ -V_{-2}(s) + V_{+3}(s) - V_{-3}(s) \end{pmatrix} \tag{3}$$

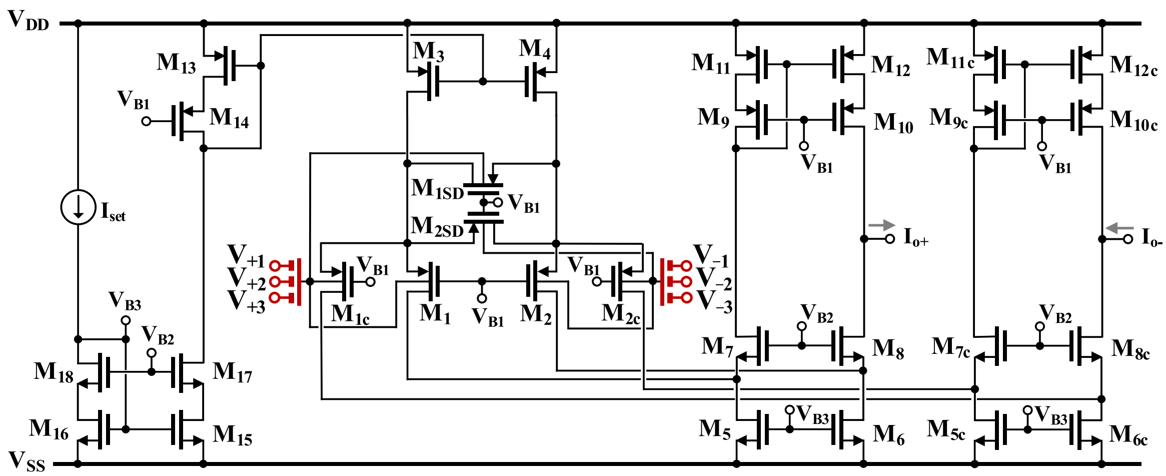

FIGURE 2. CMOS topology of the MIMO-OTA.

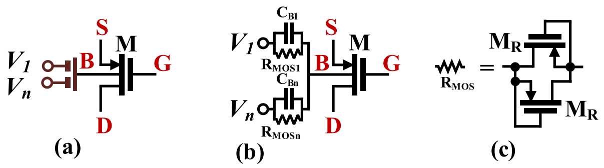

FIGURE 3. MIBD-MOST technique, (a) symbol, (b) realization, (c) R_{MOS} realization.

The core of the differential input stage (M_1, M_{1c}, M_2, M_{2c}, M_{1SD} and M_{2SD}) can be treated as a bulk-driven version of a source degenerative input stage. Its gate-driven strong-inversion version was first described in [20]. Transistors M_{1SD}, M_{2SD} operate in a triode region as resistors controlled by an input signal, which improves linearity. Here, the bulk terminal is used as the signal input, and all transistors operate in weak inversion. Such a version of the input stage was previously proposed and verified experimentally in [19]; however, in the circuit proposed in this work, the input transistors M_1 (M_2) are split into two identical devices, M_1 and M_{1c} (M_2, M_{2c}). Their drain currents are transferred to different cascode output stages, thus creating the high-impedance outputs of the OTA, I_{o+} and I_{o-}. The use of bulk terminals instead of gates extends the linear range of the OTA, as well as its common-mode range, which is especially advantageous in a low-voltage environment.

Using the results provided in [19], for frequencies above f_c, with $M_1 = M_{1c}$, $M_2 = M_{2c}$ and $I_{D3} = I_{D4} = I_{set}$, the quasi-static transfer characteristic of the OTA from the i-th input with other inputs grounded can be expressed as:

$$I_{o+} = -I_{o-} = I_{set} tanh\left(\eta\beta\frac{V_{+i} - V_{-i}}{2n_p U_T} - tanh^{-1}\left(\frac{1}{4m+1} tanh\left(\eta\beta\frac{V_{+i} - V_{-i}}{2n_p U_T}\right)\right)\right) \tag{4}$$

where $\eta = (n_p\text{-}1) = g_{mb1,2}/g_{m1,2}$ is the bulk to gate transconductance ratio at the operating point for the input transistors M_1 M_{1c}, M_2 and M_{2c}, n_p is the subthreshold slope factor for p-channel devices and U_T is the thermal potential. Assuming $M_1 = M_{1c}$ and $M_2 = M_{2c}$, the coefficient $m = (W_{1,2SD}/L_{1,2SD})/2(W_{1,2}/L_{1,2})$ is the relative aspect ratio of the two matched transistor pairs M_1, M_2 and M_{1SD}, M_{2SD}. For optimum linearity, $m = 1/2$, i.e., all the transistors M_1, M_{1c}, M_2, M_{2c}, M_{1SD} and M_{2SD} can be identical.

From (4), the small-signal transconductance of the OTA, as defined by (1), is given by:

$$g_m = \eta\beta \cdot \frac{2m}{4m+1}\frac{I_{set}}{n_p U_T} \tag{5}$$

and for the case of optimum linearity ($m = 1/2$)

$$g_m = \frac{\eta\beta}{3} \cdot \frac{I_{set}}{n_p U_T} \tag{6}$$

As we can conclude from (6), the small-signal transconductance of the OTA is attenuated η times by using the bulk terminal of the device rather than the gate, and β times by the input capacitive divider. Typically, for a weak-inversion region, three inputs, and the used technology node, the product of $\eta\beta$ is around 1/10. However, the input linear range and the input referred noise are increased proportionally. The dynamic range remains unchanged and is the same as for the gate-driven counterpart of the circuit with source degeneration.

The low transconductance value affects the DC voltage gain of the OTA; therefore, a folded-cascode topology is used to boost the gain. The DC voltage gain of the OTA can be approximated as:

$$A_{vo} = g_m \left(r_{ds8}\left(1 + g_{m8} r_{s8}\right) || r_{ds10}\left(1 + g_{m10} r_{ds12}\right)\right) \tag{7}$$

where $r_{s8} = r_{ds6}||(r_{ds2}(1+g_{m2}r_{ds2SD}/4)$.

Thus, as can be concluded from (7), the DC voltage gain of the OTA is significantly improved, thus compensating for the

TABLE 1. Obtained variant filtering functions of the proposed mixed-mode universal filter.

Mode	Function		Input	Output
VM	LPF	Non-inverting	V_{i5}	V_{o1}
		Inverting	V_{i6}	V_{o1}
	BPF	Non-inverting	V_{i3}	V_{o1}
		Inverting	V_{i4}	V_{o1}
	HPF	Non-inverting	V_{i1}	V_{o1}
		Inverting	V_{i2}	V_{o1}
	BSF	Non-inverting	V_{i1}=V_{i5}	V_{o1}
		Inverting	V_{i2}=V_{i6}	V_{o1}
	APF	Non-inverting	V_{i1}=V_{i4}=V_{i5}	V_{o1}
		Inverting	V_{i2}=V_{i3}=V_{i6}	V_{o1}
TAM	LPF	Non-inverting	V_{i5}	I_{o1}
		Inverting	V_{i6}	I_{o1}
	BPF	Non-inverting	V_{i3}	I_{o1}
		Inverting	V_{i4}	I_{o1}
	HPF	Non-inverting	V_{i1}	I_{o1}
		Inverting	V_{i2}	I_{o1}
	BSF	Non-inverting	V_{i1}=V_{i5}	I_{o1}
		Inverting	V_{i2}=V_{i6}	I_{o1}
	APF	Non-inverting	V_{i1}=V_{i4}=V_{i5}	I_{o1}
		Inverting	V_{i2}=V_{i3}=V_{i6}	I_{o1}
CM	LPF	Inverting	I_{i3}	I_{o1}
		Non-inverting	I_{i3}	I_{o2}
	BPF	Inverting	I_{i2}	I_{o2}
		Non-inverting	I_{i2}	I_{o1}
	HPF	Inverting	I_{i1}	I_{o1}
		Non-inverting	I_{i1}	I_{o2}
	BSF	Inverting	I_{i1}=I_{i3}	I_{o1}
		Non-inverting	I_{i1}=I_{i3}	I_{o2}
	APF	Inverting	I_{i1}=I_{i2}=I_{i3}	I_{o1}
		Non-inverting	I_{i1}=I_{i2}=I_{i3}	I_{o2}
TIM	LPF	Inverting	I_{i3}	V_{o1}
		Non-inverting	I_{i3}	V_{o2}
	BPF	Inverting	I_{i2}	V_{o2}
		Non-inverting	I_{i2}	V_{o1}
	HPF	Inverting	I_{i1}	V_{o1}
		Non-inverting	I_{i1}	V_{o2}
	BSF	Inverting	I_{i1}=I_{i3}	V_{o1}
		Non-inverting	I_{i1}=I_{i3}	V_{o2}
	APF	Inverting	I_{i1}=I_{i2}=I_{i3}	V_{o1}
		Non-inverting	I_{i1}=I_{i2}=I_{i3}	V_{o2}

gain loss from the input capacitive divider and the bulk-driven technique.

III. PROPOSED MIXED-MODE ACTIVE FILTER

Fig. 4 shows the proposed mixed-mode active filter employing three MI-OTAs, one MIMO-OTA, two grounded capacitors, and one grounded resistor. The multiple-input voltage mode of the OTA offers many non-inverting and inverting voltage-mode transfer functions, and the multiple-output of the OTA offers easy non-inverting and inverting current-mode transfer functions. The use of grounded passive components is ideal for integrated circuits.

Using (1) and nodal analysis, the outputs V_{o1}, I_{o1}, V_{o2}, I_{o2} can be given by

$$V_{o1} = \frac{s^2C_1C_2\left(V_{i1} - V_{i2}\right) + sC_1g_{m2}\left(V_{i3} - V_{i4}\right) + g_{m1}g_{m2}\left(V_{i5} - V_{i6}\right)}{s^2C_1C_2 + sC_1g_{m2} + g_{m1}g_{m2}} \quad (8)$$

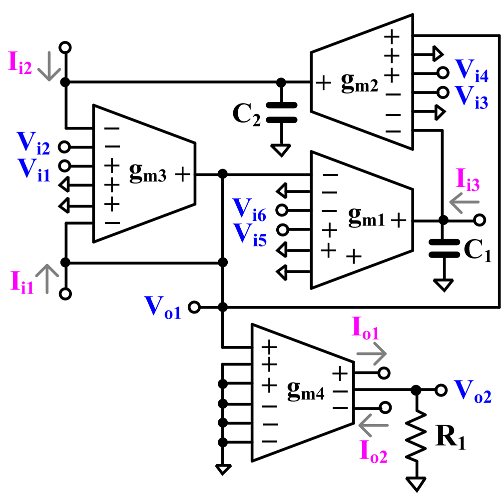

FIGURE 4. Proposed mixed-mode active filter.

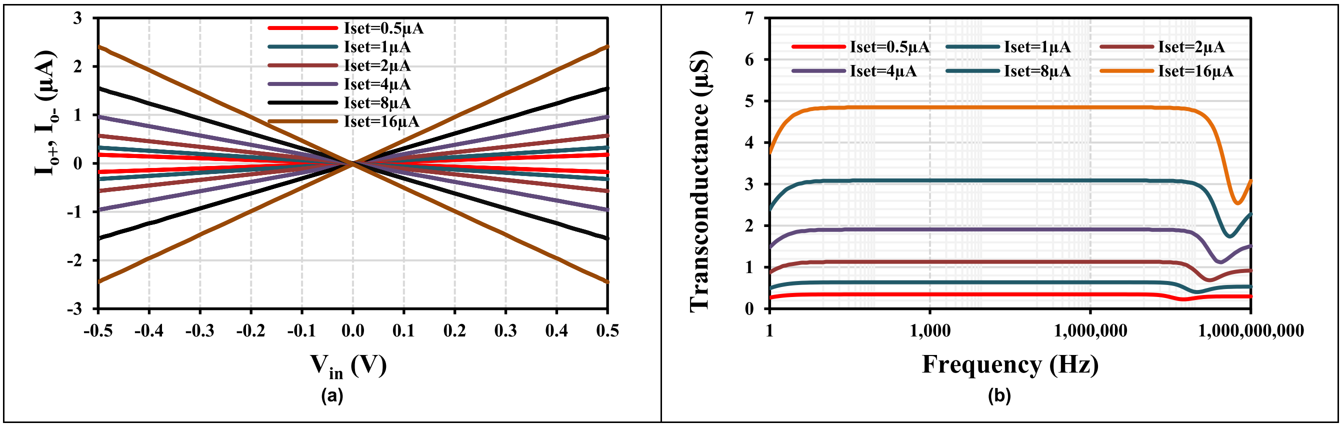

FIGURE 5. a) The output current I_{o+} (solid line), I_{o-} (dashed line) versus the input voltage V_{in}, and b) the transconductance frequency characteristics with different setting currents.

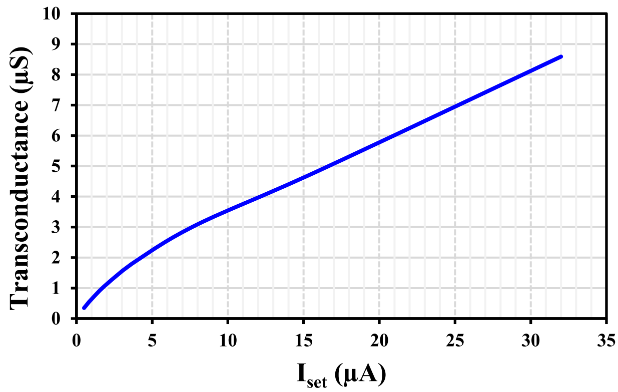

FIGURE 6. The transconductance versus the setting current.

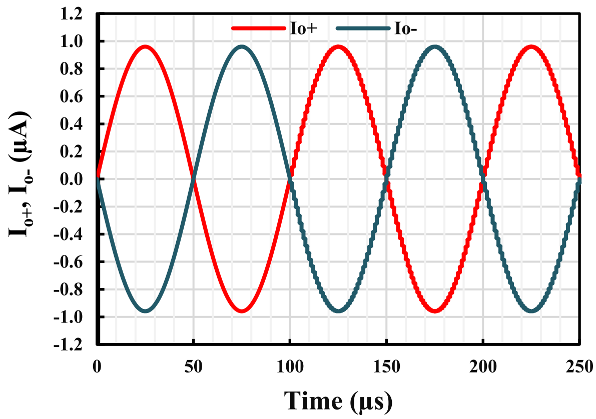

FIGURE 8. The transient response of the output currents of the MIMO-OTA with applied sine wave signal with 500mV amplitude at 10 kHz and setting current $I_{set} = 4\ \mu A$.

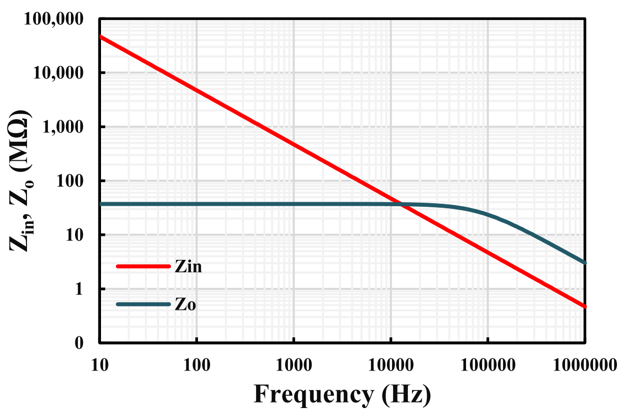

FIGURE 7. The frequency characteristics of the input and output impedance of the proposed MIMO-OTA with setting current $I_{set} = 4\ \mu A$.

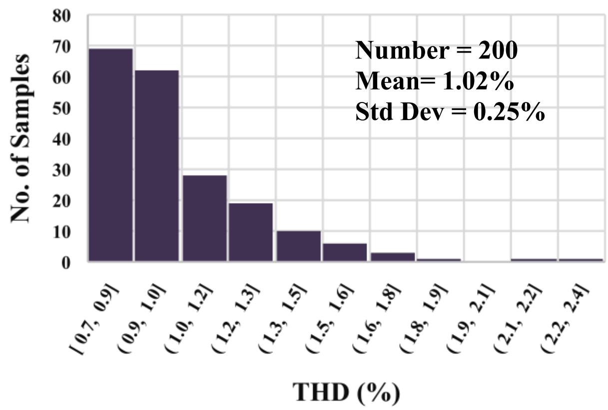

FIGURE 9. The histogram of the output current's THD with setting current $I_{set} = 4\ \mu A$ based on MC process and mismatch analysis.

$$I_{o1} = g_{m4}\left(\frac{s^2C_1C_2\left(V_{i1}-V_{i2}\right)+sC_1g_{m2}\left(V_{i3}-V_{i4}\right)+g_{m1}g_{m2}\left(V_{i5}-V_{i6}\right)}{s^2C_1C_2+sC_1g_{m2}+g_{m1}g_{m2}}\right) \tag{9}$$

$$I_{o1} = \frac{g_{m4}}{g_{m3}}\left(\frac{-s^2C_1C_2I_{i1}+sC_1g_{m3}I_{i2}-g_{m2}g_{m3}I_{i3}}{s^2C_1C_2+sC_1g_{m2}+g_{m1}g_{m2}}\right) \tag{10}$$

$$I_{o2} = \frac{g_{m4}}{g_{m3}}\left(\frac{s^2C_1C_2I_{i1}-sC_1g_{m3}I_{i2}+g_{m2}g_{m3}I_{i3}}{s^2C_1C_2+sC_1g_{m2}+g_{m1}g_{m2}}\right) \tag{11}$$

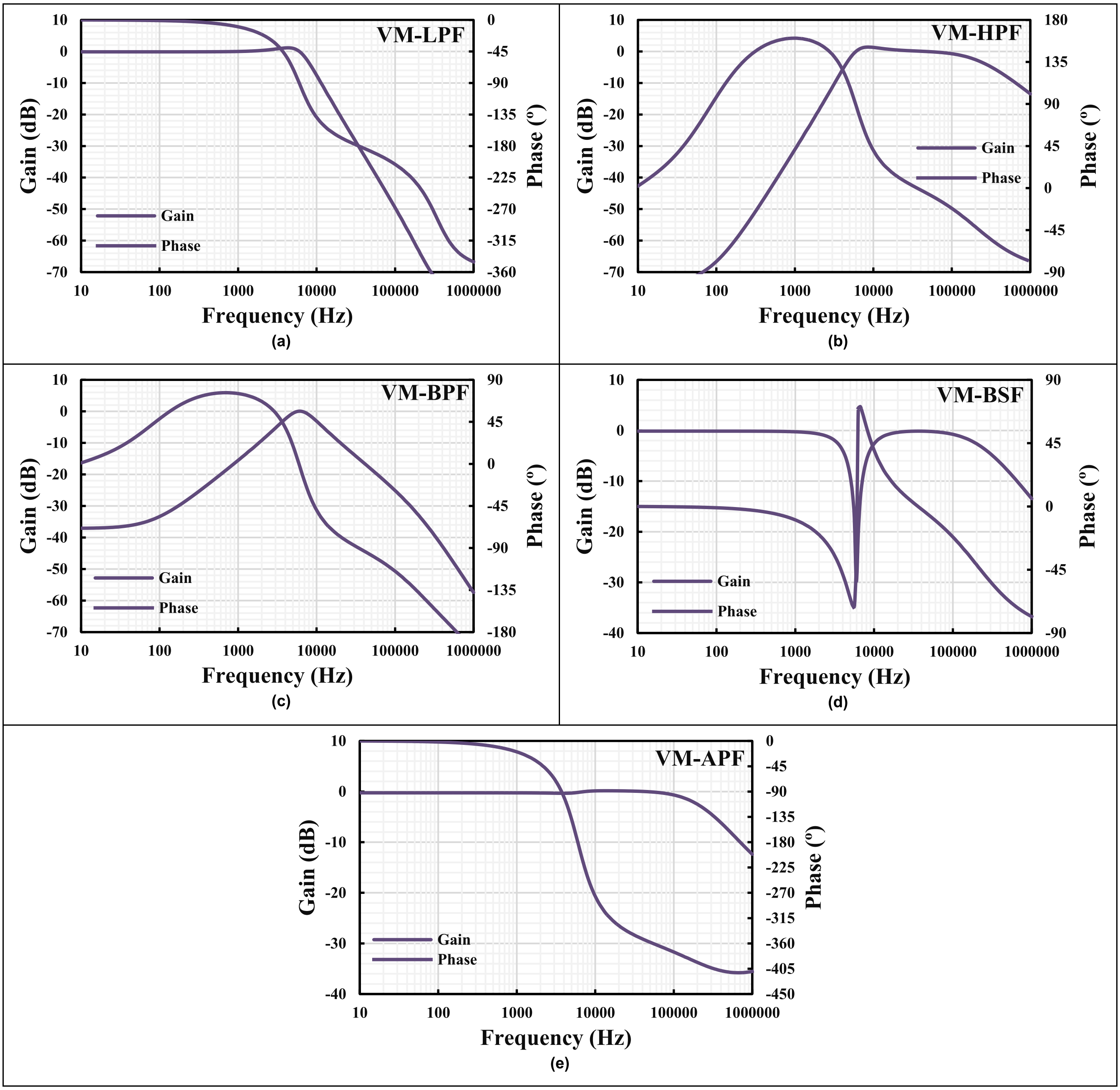

FIGURE 10. VM filter magnitude and phase responses with setting current $I_{set} = 4\ \mu A$ for: a) LPF, b) HPF, c) BPF, d) BSF and e) APF.

$$V_{o1} = \frac{1}{g_{m3}}\left(\frac{-s^2C_1C_2I_{i1} + sC_1g_{m3}I_{i2} - g_{m2}g_{m3}I_{i3}}{s^2C_1C_2 + sC_1g_{m2} + g_{m1}g_{m2}}\right) \quad (12)$$

$$V_{o2} = \frac{g_{m4}R_1}{g_{m3}}\left(\frac{s^2C_1C_2I_{i1} - sC_1g_{m3}I_{i2} + g_{m2}g_{m3}I_{i3}}{s^2C_1C_2 + sC_1g_{m2} + g_{m1}g_{m2}}\right) \quad (13)$$

Letting $g_{m4} = 1/R_1$, the obtained variant filtering functions are given in Table 1. It is evident that both non-inverting and inverting filtering functions of LPF, HPF, BPF, BSF, and APF can be obtained in VM, CM, TAM, and TIM in single topology by selecting appropriate input and output signals. Thus, 40 transfer function can be obtained, providing full capability of the mixed-mode filter.

The natural frequency (ω_o) and the quality factor (Q) can be respectively expressed by

$$\omega_o = \sqrt{\frac{g_{m1}g_{m2}}{C_1C_2}} \quad (14)$$

$$Q = \sqrt{\frac{g_{m1}C_2}{g_{m2}C_1}} \quad (15)$$

The parameter ω_o can be electronically controlled by g_{m1} and g_{m2} and the parameter Q can be given by C_2/C_1. The

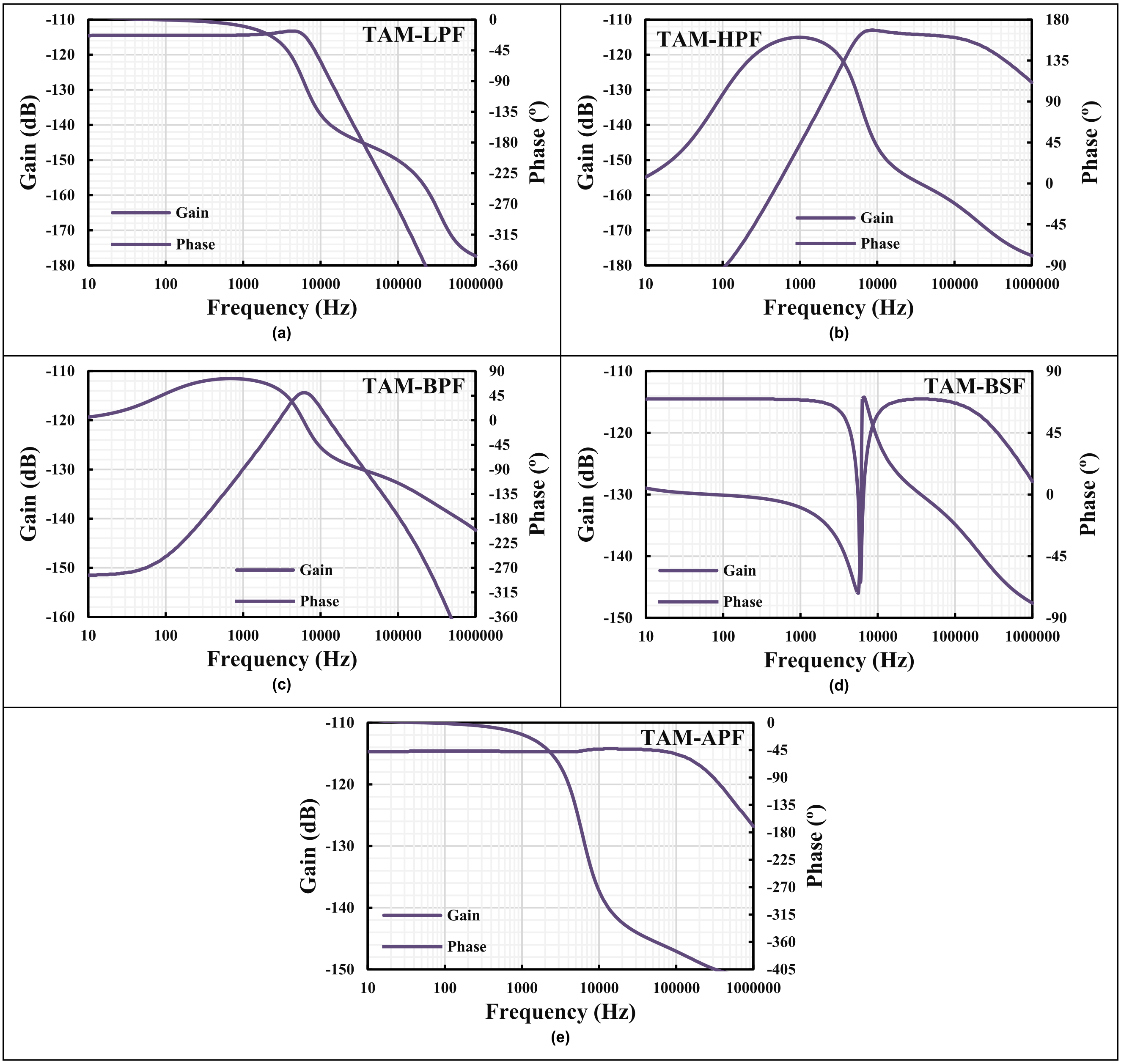

FIGURE 11. TAM filter magnitude (solid line) and phase (dashed line) responses with $I_{set} = 4\ \mu A$ for: a) LPF, b) HPF, c) BPF, d) BSF and e) APF.

study of the effect of the OTA's non-idealities on the proposed filter's (Fig. 4) performance is shown below. Using the practical small signal OTA model in [21], there are three components taken into consideration: (i) the differential-mode capacitance C_d, and common-mode capacitance C_c, (ii) the output capacitance C_o and output conductance g_o, and (iii) the frequency-dependent transconductance that can be given [21] by

$$g_m(s) \approx g_{mo}(1 - s\tau) \tag{16}$$

where g_{mo} is the transconductance of the ideal OTA, $\tau = 1/\omega_g$, and ω_g is the second pole of the OTA which is given by the cut-off frequency of the OTA.

The frequency-dependent transconductance in (17) has been included in this consideration. The denominator of the proposed filter can be expressed by

$$s^2 C_1 C_2 \left(1 - \frac{C_1 g_{mo2}\tau_2 - g_{mo1} g_{mo2}\tau_1\tau_2}{C_1 C_2}\right) + sC_1 g_{mo2}\left(1 - \frac{g_{mo1} g_{mo2}\tau_1 + g_{mo1} g_{mo2}\tau_2}{C_1 g_{mo2}}\right) + g_{mo1} g_{mo2} \tag{17}$$

The effect of frequency-dependent transconductance can be made negligible by satisfying the following

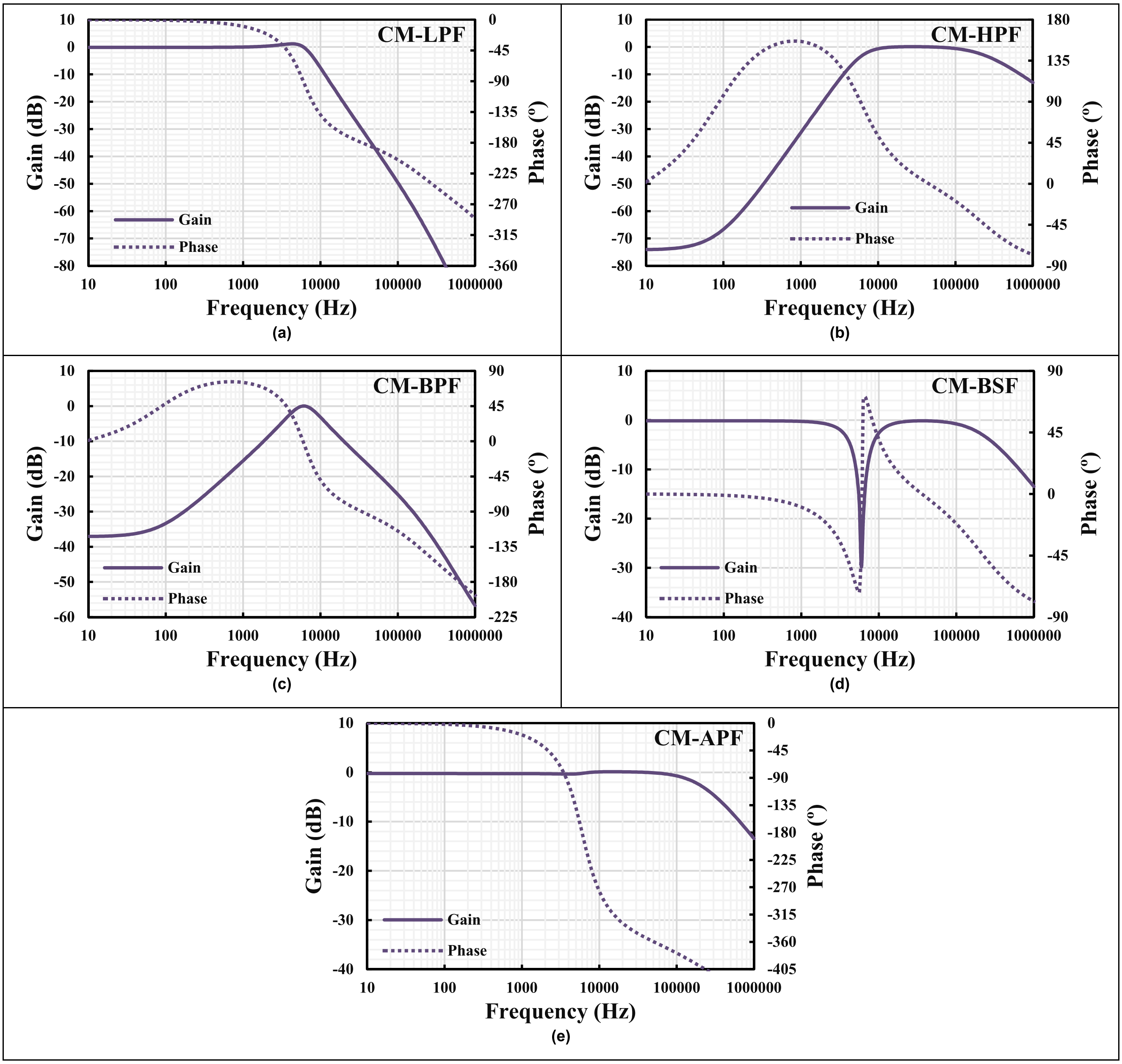

FIGURE 12. CM filter magnitude (solid line) and phase (dashed line) responses with $I_{set} = 4\ \mu A$ for: a) LPF, b) HPF, c) BPF, d) BSF and e) APF.

conditions:

$$\frac{C_1 g_{mo2}\tau_2 - g_{mo1}g_{mo2}\tau_1\tau_2}{C_1C_2} \ll 1 \tag{18}$$

$$\frac{g_{mo1}g_{mo2}\tau_1 + g_{mo1}g_{mo2}\tau_2}{C_1 g_{mo2}} \ll 1 \tag{19}$$

Considering the parasitic parameters in Fig. 4, the parasitic capacitances C_{o1}, C_{c2} and parasitic conductance g_{o1} are parallel with C_1, and the parasitic capacitances C_{o2}, C_{c3} and parasitic conductance g_{o2} are parallel with C_2. C_{o1} and C_{o2} are respectively the output capacitances of g_{m1} and g_{m2}, C_{c1} and C_{c2} are respectively the common-mode capacitances of g_{m1} and g_{m2}, and g_{o1} and g_{o2} are respectively the output conductances of g_{m1} and g_{m2}. The parasitic capacitances and conductances can be neglected by choosing appropriate values, such as $C_1 \gg C_{o1}+C_{c2}$, $C_2 \gg C_{o2}+C_{c3}$, $g_{m1} \gg g_{o1}$, $g_{m2} \gg g_{o2}$.

IV. SIMULATION RESULTS

The Cadence Virtuoso System Design Platform using 0.18 μm CMOS technology from TSMC (Taiwan Semiconductor Manufacturing Company) was used for designing and simulating the proposed MIMO-OTA and the filter. The aspect ratio of the MOS transistors of the MIMO-OTA shown in Fig. 2 is listed in Table 2. The supply voltage was

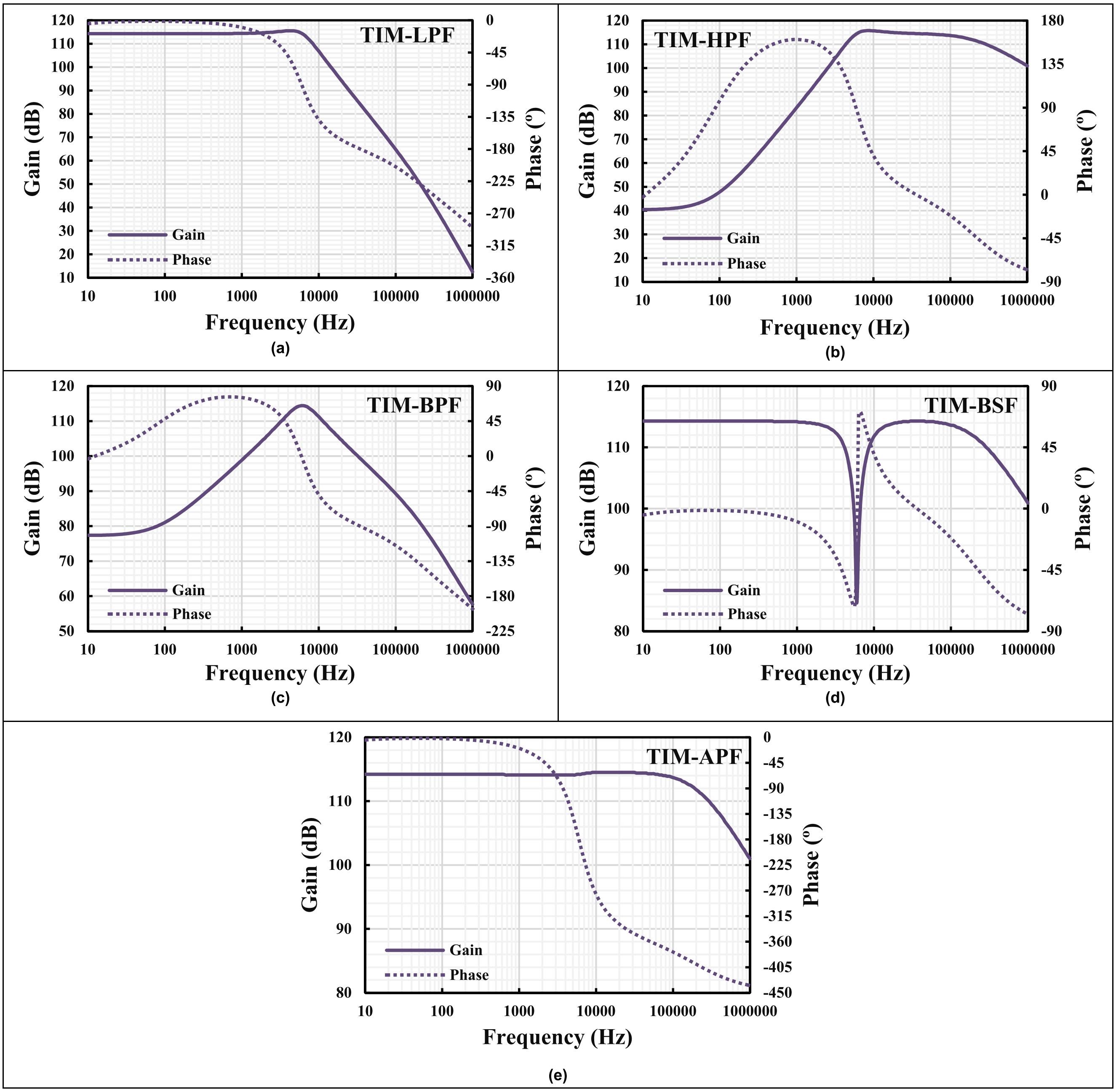

FIGURE 13. TIM filter magnitude (solid line) and phase (dashed line) responses with $I_{set} = 4\ \mu A$ for: a) LPF, b) HPF, c) BPF, d) BSF and e) APF.

$V_{DD} = -V_{SS} = 0.5$ V and the power consumption of the MIMO-OTA with two current outputs (I_{o+}, I_{o-}) was 39.2 μW for $I_{set} = 4\ \mu$A.

The output currents I_{o+}, I_{o-} versus input voltage V_{in} of the proposed MIMO-OTA for different setting currents $I_{set} = (0.5, 1, 2, 4, 8, 16)\ \mu$A are shown in Fig. 5 (a). These curves are obtained by applying an input sine wave signal with a 500 mV amplitude and 10 kHz frequency. Operation capability with a wide input voltage range is evident. The transconductance frequency characteristics for different setting currents are shown in Fig. 5 (b).

TABLE 2. Parameters of the MIMO-OTA's components.

Transistor	W/L (µm/ µm)
M_1, M_2, M_{1c}, M_{2c}	10/0.5
M_{1SD}, M_{2SD}	2.5/0.5
M_{13}- M_{18}	10/0.5
M_5-M_{12}, M_{5c}-M_{12c}	20/0.5
M_{b1}, M_{b2}	4/5
C_b=0.5 pF	
V_{B1}= –300mV, V_{B2}=200mV	

The transconductance values at 10 kHz frequency obtained from Fig. 5 (b) versus setting current I_{set} is shown in Fig. 6.

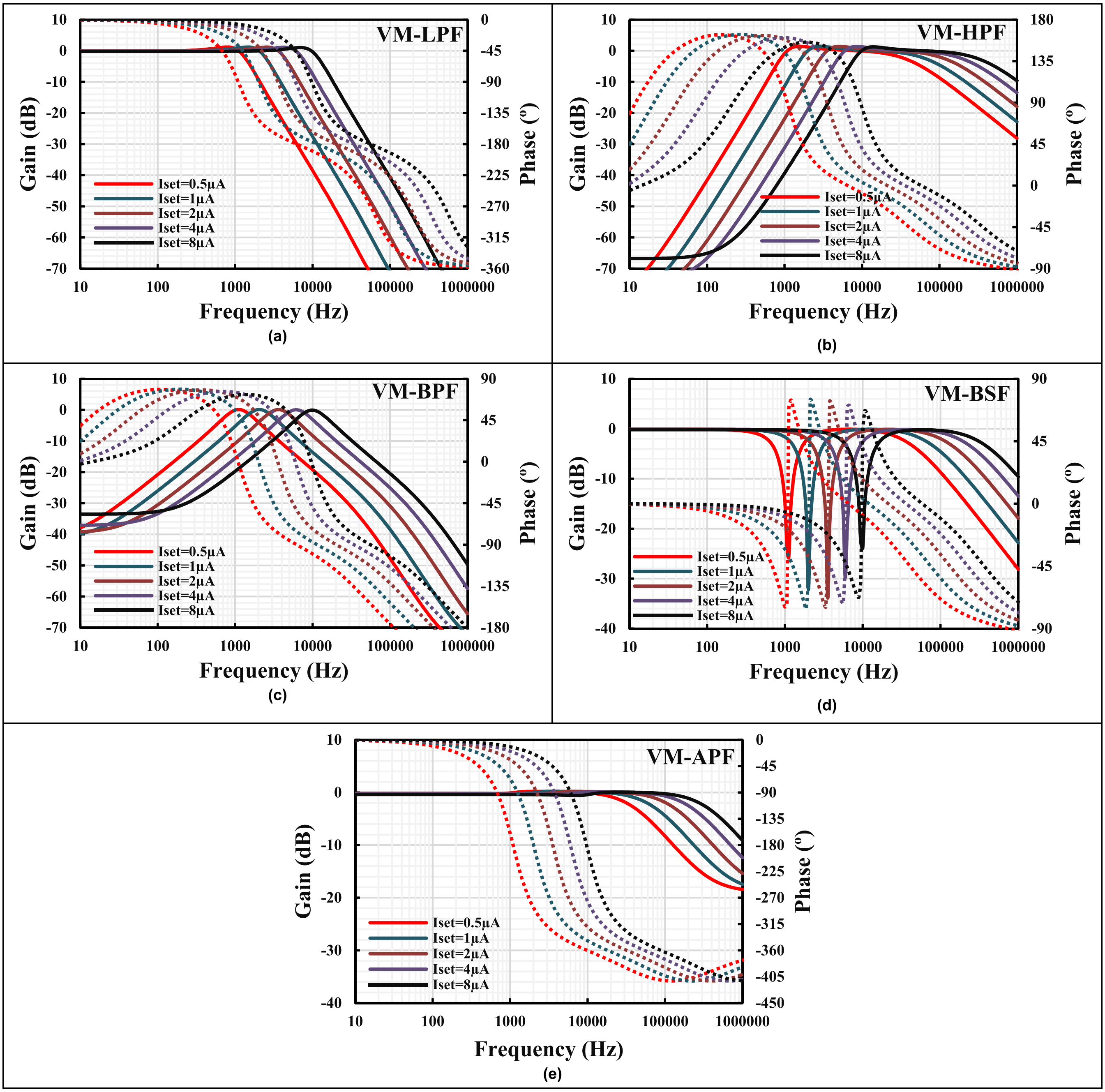

FIGURE 14. VM filter magnitude (solid line) and phase (dashed line) responses with various setting current I_{set} = (0.5, 1, 2, 4, 8) μA for: a) LPF, b) HPF, c) BPF, d) BSF and e) APF.

As is evident, the wide turnability of the transconductance is confirmed.

The process, voltage, and temperature corners analysis (PVT) show an acceptable variance of the transconductance value, where the nominal value at 10 kHz is 1.84 μS for I_{set} = 4 μA as shown in Fig. 5 (b). The process corners take into account the variation of the MOS transistor (fast-fast, fast-slow, slow-fast, slow-slow) and also the variation of the MIM capacitor (fast-fast, slow-slow). The value of the transconductance varied from 1.84 μS to 1.93 μS. For the voltage corners ($V_{DD}\pm10\%V_{DD}$), the value of the transconductance varied from 1.901 μS to 1.907 μS. For the temperature corners ($-20°$ C, $70°$ C), the value of the transconductance varied from 1.62 μS to 2.07 μS. All these variances are acceptable.

The frequency characteristics of the input and output impedance of the proposed MIMO-OTA with setting current I_{set} = 4 μA are shown in Fig. 7. The input impedance at low frequencies was high at 330 GΩ. The output impedance

TABLE 3. Properties comparison of this work with those of mixed-mode universal filters.

Factor	Proposed	[11]	[12]	[13]	[15]	[16]
Number of active devices	4-OTA	5-OTA	8-OTA	4-OTA	5-OTA	6-OTA
Realization	0.18 µm CMOS	0.18 µm CMOS	0.18 µm CMOS	0.18 µm CMOS	Commercial IC (LT1228)	0.18 µm CMOS
Number passive devices	2-C, 1-R	2-C	2-C	2-C	2-C	2-C
Type of filter	MIMO	MISO	MIMO	MIMO	MIMO	SIMO
Total number of offered responses	40	20	20	35	7	20
Each mode offered non-inverting and inverting responses	Yes	No	No	No	No	No
Power supply (V)	±0.5	±0.9	±0.3	0.5	-	±0.5
Power dissipation (µW)	156.8	177.3	5.77	58	-	75
Natural frequency (kHz)	5.95	3.39×10^3	5	114×10^{-3}	159.16	1.5×10^3
Total harmonic distortion (%)	1@220mV	-	<2@200mV$_{pp}$	1@170mV$_{pp}$	-	4@310mV
Dynamic range (dB)	40.2	-	53.2	53.2	-	-
Verification of result	Sim	Sim	Sim	Sim	Sim/Exp	Sim

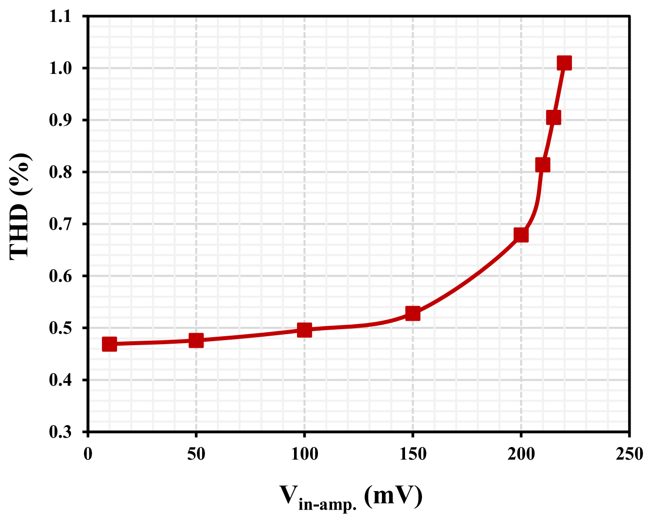

FIGURE 15. The THD versus the amplitude of input signal at 1 kHz for $I_{set} = 4\ \mu$A of the VM LPF.

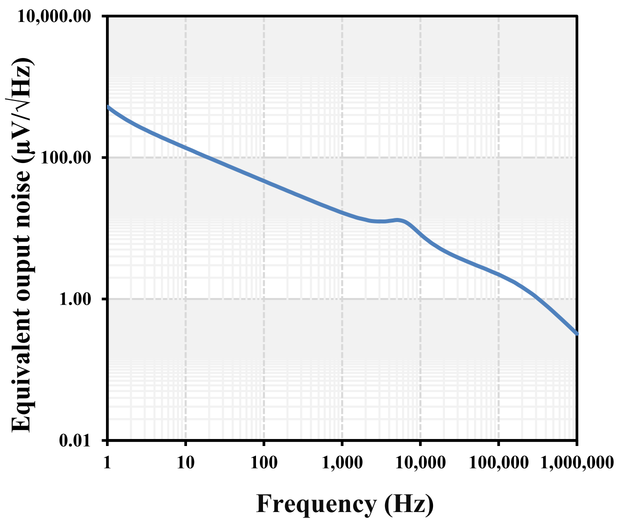

FIGURE 16. The equivalent output noise of the VM LPF for $I_{set} = 4\ \mu$A.

value reached 35.9 MΩ due to the cascode structure. The transient response of the output currents I_{o+} and I_{o-} of the MIMO-OTA with the setting current $I_{set} = 4\ \mu$A is shown in Fig. 8. A sine wave signal with an amplitude of 500 mV at a frequency of 10 kHz was applied to the MIMO-OTA input. The THD the output currents I_{o+} and I_{o-} was approximately 0.8 %. The histogram of the THD of the output current obtained by Monte-Carlo (MC) process and mismatch analysis at 200 runs and at setting current $I_{set} = 4\ \mu$A is shown in Fig. 9. The mean value of the THD was 1.02 %, the minimum value was 0.7 %, the maximum value was 2.3 % and the standard deviation was 0.25 **%.** The simulation was obtained for applied input sine signal with a 500 mV amplitude and 10 kHz frequency. This indicates that the MIMO-OTA can operate with rail-to-rail signal and low THD at around 1 %.

The functionality of the filter was confirmed by simulation. The simulation results of the mixed-mode filter are presented in Figs. 10-13. Fig. 10 shows the magnitude and phase responses of the non-inverting VM filter with $C_1 = C_2 = 50$ pF and setting current $I_{set} = I_{set1-4} = 4\ \mu$ A for a) LPF, b) HPF, c) BPF, d) BSF and e) APF. The cutoff frequency was 5.95 kHz. The power consumption of the filter was $4 \times 39.2\ \mu W = 156.8\ \mu W$. Under the same input conditions used to obtain the results in Fig. 10, the magnitude and phase responses of the non-inverting TAM filter can be seen Fig. 11. Thus, the non-inverting mode of the LPF, HPF, BPF, BSP, APF can be obtained in VM/TAM. If the opposite input conditions are used, the magnitude and phase responses of the inverting VM/TAM can be obtained. This is already expressed in Table 1. Thanks to the multiple-input OTA (i.e., g_{m1}, g_{m2}, g_{m3}), non-inverting/inverting VM/TAM filters can be easily obtained.

Figs. 12 and 13 show the magnitude and phase responses, respectively, of the non-inverting CM/TAM with $I_{set} = 4\ \mu$A for a) LPF, b) HPF, c) BPF, d) BSF and e) APF. Thanks to the multiple-output OTA (i.e., g_{m4}), the output I_{o2} is the inverted signal of output I_{o1} and the output V_{o2} is the inverted signal of the output V_{o1}. Thus, if the output conditions are opposite to those used to obtain the results in Figs. 12 and 13, the magnitude and phase responses of the inverting VM/TAM can be obtained. This is already expressed in Table 1. When V_{o2} is used, $g_{m4} = 1/R_1$ can be used to obtain $V_{o2} = -V_{o1}$.

To demonstrate the filter's tuning capabilities, Fig. 14 shows the magnitude and phase responses for different setting currents $I_{set} = (0.5, 1, 2, 4, 8)$ μA. The cutoff frequencies were (1.12, 1.99, 3.54, 5.95, 10) kHz, respectively. This frequency range is sufficient for low frequency applications, such as bio-signal processing.

The total harmonic distortion (THD) versus the amplitude of the input sine wave signal at 1 kHz for $I_{set} = 4$ μA for the VM LPF is shown in Fig. 15. The THD was 1% for the 220 mV input signal. The equivalent output noise of the VM LPF for $I_{set} = 4$ μA is shown in Fig. 16. The integrated output noise in the 1Hz-5.95kHz band was 1.528mV. This results in a dynamic range (DR) of 40.2 dB for 1 % THD.

The proposed mixed-mode active filter is compared with some previous works in Table 3. The mixed-mode universal filters using OTA as active elements in [11], [12], [13], [15], and [16] were used to compare. It is clear that the multiple-input multiple-output OTA based mixed-mode filter can offer maximum transfer functions. Compared with [11], [12], [13], [15], and [16], the proposed filter offers the full capability of a mixed-mode filter, namely all VM, TAM, CM, and TIM offer both non-inverting and inverting transfer functions of LP, HP, BP, BS, and AP filters. Compared with [11], [12], [15], and [16], the proposed filter employs a minimum number of active OTAs.

V. CONCLUSION

This work introduces a new mixed-mode active filter using multiple-input multiple-output OTAs as active devices. The OTA with multiple non-inverting/inverting input voltage terminals facilitates the attainment of non-inverting/inverting filtering functions without additional circuitry (i.e., inverting amplifiers) when used in active filters. Furthermore, the OTA with multiple plus/minus current output terminals enables easy to obtain non-inverting/inverting current-mode transfer functions. The proposed mixed-mode active filter employs three MI-OTAs, one MIMO-OTA, two grounded capacitors, and one grounded resistor. The proposed mixed-mode filter offers VM, CM, TAM, and TIM in the same circuit and each mode of operation provides both non-inverting and inverting transfer functions of LPF, HPF, BPF, BSF, APF. Thus, the proposed filter offers 40 transfer functions, which is the full capability of a mixed universal filter. The natural frequency of all filtering functions can be electronically controlled. The filter uses 1-V of supply voltage, consumes 156.8 μW of power, and has a 40.2 dB dynamic range.

REFERENCES

[1] V. K. Singh, A. K. Singh, D. R. Bhaskar, and R. Senani, "Novel mixed-mode universal biquad configuration," *IEICE Electron. Exp.*, vol. 2, no. 22, pp. 548–553, 2005, doi: 10.1587/elex.2.548.

[2] D. R. Bhaskar, A. Raj, R. Senani, and P. Kumar, "CFOA-based simple mixed-mode first-order universal filter configurations," *Int. J. Circuit Theory Appl.*, vol. 50, no. 7, pp. 2631–2641, Jul. 2022, doi: 10.1002/cta.3289.

[3] M. T. Abuelma'atti, A. Bentrcia, and S. M. Al-Shahrani, "A novel mixed-mode current-conveyor-based filter," *Int. J. Electron.*, vol. 91, no. 3, pp. 191–197, Mar. 2004, doi: 10.1080/00207210410001677039.

[4] K. Ghosh and B. N. Ray, "CCII-based nth-order mixed mode elliptic filter with grounded R and C," *J. Circuits, Syst. Comput.*, vol. 24, no. 3, Mar. 2015, Art. no. 1550035, doi: 10.1142/s0218126615500358.

[5] C.-M. Chang, C.-N. Lee, C.-L. Hou, J.-W. Horng, and C.-K. Tu, "High-order DDCC-based general mixed-mode universal filter," *IEE Proc. Circuits, Devices Syst.*, vol. 153, no. 5, p. 511, 2006, doi: 10.1049/ip-cds:20050345.

[6] C.-N. Lee, "Independently tunable mixed-mode universal biquad filter with versatile input/output functions," *AEU Int. J. Electron. Commun.*, vol. 70, no. 8, pp. 1006–1019, Aug. 2016, doi: 10.1016/j.aeue.2016.04.006.

[7] M. T. Abuelma'atti and A. Bentrcia, "A novel mix ed-mode OTA-C universal filter," *Int. J. Electron.*, vol. 92, pp. 375–383, 2005, doi: 10.1080/08827510412331295009.

[8] C.-N. Lee and C.-M. Chang, "High-order mixed-mode OTA-C universal filter," *AEU Int. J. Electron. Commun.*, vol. 63, no. 6, pp. 517–521, Jun. 2009, doi: 10.1016/j.aeue.2008.04.004.

[9] H.-P. Chen, Y.-Z. Liao, and W.-T. Lee, "Tunable mixed-mode OTA-C universal filter," *Anal. Integr. Circuits Signal Process.*, vol. 58, no. 2, pp. 135–141, Feb. 2009, doi: 10.1007/s10470-008-9228-z.

[10] M. Parvizi, "Design of a new low power MISO multi-mode universal biquad OTA-C filter," *Int. J. Electron.*, vol. 106, no. 3, pp. 440–454, Mar. 2019, doi: 10.1080/00207217.2018.1540064.

[11] D. R. Bhaskar, A. Raj, and P. Kumar, "Mixed-mode universal biquad filter using OTAs," *J. Circuits, Syst. Comput.*, vol. 29, Apr. 2020, Art. no. 2050162.

[12] A. Namdari and M. Dolatshahi, "Design of a low-voltage and low-power, reconfigurable universal OTA-C filter," *Anal. Integr. Circuits Signal Process.*, vol. 111, no. 2, pp. 169–188, May 2022, doi: 10.1007/s10470-022-01996-2.

[13] F. Khateb, M. Kumngern, and T. Kulej, "58-nW 0.5-V mixed-mode universal filter using multiple-input multiple-output OTAs," *IEEE Access*, vol. 11, pp. 130345–130357, 2023, doi: 10.1109/ACCESS.2023.3332992.

[14] A. Namdari, M. Dolatshahi, and M. Aghababaei Horestani, "A new ultra-low-power high-order universal OTA-C filter based on CMOS double inverters in the subthreshold region," *Circuits, Syst., Signal Process.*, vol. 42, no. 11, pp. 6379–6398, Nov. 2023, doi: 10.1007/s00034-023-02401-7.

[15] S.-F. Wang, H.-P. Chen, Y. Ku, and Y.-C. Lin, "Versatile tunable voltage-mode biquadratic filter and its application in quadrature oscillator," *Sensors*, vol. 19, no. 10, p. 2349, May 2019, doi: 10.3390/s19102349.

[16] M. Parvizi, A. Taghizadeh, H. Mahmoodian, and Z. D. Kozehkanani, "A low-power mixed-mode SIMO universal Gm–C filter," *J. Circuits, Syst. Comput.*, vol. 26, no. 10, Oct. 2017, Art. no. 1750164, doi: 10.1142/s021812661750164x.

[17] C.-N. Lee, "Fully cascadable mixed-mode universal filter biquad using DDCCS and grounded passive components," *J. Circuits, Syst. Comput.*, vol. 20, no. 4, pp. 607–620, Jun. 2011, doi: 10.1142/s0218126611007499.

[18] F. Khateb, T. Kulej, M. Kumngern, and C. Psychalinos, "Multiple-input bulk-driven MOS transistor for low-voltage low-frequency applications," *Circuits, Syst., Signal Process.*, vol. 38, no. 6, pp. 2829–2845, Jun. 2019, doi: 10.1007/s00034-018-0999-x.

[19] F. Khateb, T. Kulej, M. Akbari, and K.-T. Tang, "A 0.5-V multiple-input bulk-driven OTA in 0.18-μm CMOS," *IEEE Trans. Very Large Scale Integr. (VLSI) Syst.*, vol. 30, no. 11, pp. 1739–1747, Nov. 2022, doi: 10.1109/TVLSI.2022.3203148.

[20] F. Krummenacher and N. Joehl, "A 4-MHz CMOS continuous-time filter with on-chip automatic tuning," *IEEE J. Solid-State Circuits*, vols. SSC–23, no. 3, pp. 750–758, Jun. 1988, doi: 10.1109/4.315.

[21] H. Pevarez-Lozano and E. Sanchez-Sinencio, "Minimum parasitic effects biquadratic OTA-C filter architectures," *Anal. Integr. Circuits Signal Process.*, vol. 1, no. 4, pp. 297–319, Dec. 1991, doi: 10.1007/bf00239678.

MONTREE KUMNGERN received the B.S. (Ind.Ed.) degree in electrical engineering from the King Mongkut's University of Technology Thonburi, Thailand, in 1998, and the M.Eng. and D.Eng. degrees in electrical engineering from the King Mongkut's Institute of Technology Ladkrabang, Thailand, in 2002 and 2006, respectively. In 2007, he was a Lecturer with the Department of Telecommunications Engineering, Faculty of Engineering, King Mongkut's Institute of Technology Ladkrabang. From 2010 to 2017, he was an Assistant Professor. He is currently an Associate Professor. He has authored or coauthored over 200 publications in journals and proceedings of international conferences. His research interests include analog and digital integrated circuits, discrete-time analog filters, non-linear circuits, data converters, and ultra-low voltage building blocks for biomedical applications.

FABIAN KHATEB received the M.Sc. and Ph.D. degrees in electrical engineering and communication and the M.Sc. and Ph.D. degrees in business and management from Brno University of Technology, Czech Republic, in 2002, 2005, 2003, and 2007, respectively. He is currently a Professor with the Department of Microelectronics, Faculty of Electrical Engineering and Communication, Brno University of Technology; Department of Electrical Engineering, University of Defence, Brno; and Department of Information and Communication Technology in Medicine, Faculty of Biomedical Engineering, Czech Technical University in Prague. He holds five patents. He has authored or coauthored over 140 publications in journals and proceedings of international conferences. His expertise is in new principles of designing low-voltage low-power analog circuits, particularly for biomedical applications. He is a member of the Editorial Board of the *Microelectronics Journal*, *Sensor*, *Machines*, and *Electronics and Journal of Low Power Electronics and Applications*. He is an Associate Editor of IEEE ACCESS, *Circuits, Systems and Signal Processing*, *IET Circuits, Devices & Systems*, and *International Journal of Electronics*. He was a Lead Guest Editor of the Special Issues on Low Voltage Integrated Circuits and Systems on Circuits, Systems and Signal Processing, in 2017, *IET Circuits Devices & Systems*, in 2018, and *Microelectronics Journal*, in 2019. He was also a Guest Editor of the Special Issue on Current-Mode Circuits and Systems; Recent Advances, Design and Applications on *International Journal of Electronics and Communications*, in 2017.

TOMASZ KULEJ received the M.Sc. and Ph.D. degrees from Gdańsk University of Technology, Gdańsk, Poland, in 1990 and 1996, respectively. He was a Senior Design Analysis Engineer with Polish Branch of Chipworks Inc., Ottawa, Canada. He is currently an Associate Professor with the Department of Electrical Engineering, Częstochowa University of Technology, Poland, where he conducts lectures on electronics fundamentals, analog circuits, and computer aided design. He has authored or coauthored over 100 publications in peer-reviewed journals and conferences. He holds three patents. His recent research interests include analog integrated circuits in CMOS technology, with an emphasis on low voltage and low power solutions. He serves as an Associate Editor of the *Circuits Systems and Signal Processing*. He was also a Guest Editor of the Special Issues on Low Voltage Integrated Circuits on Circuits Systems and Signal Processing, in 2017, *IET Circuits Devices & Systems*, in 2018, and *Microelectronics Journal*, in 2019.